DIAGNOSTICS FOR ENERGETIC CHARGED PARTICLES RELATED TO FAST IGNITOR EXPERIMENTS

For invited volumes

Yoneyoshi Kitagawa, Kunioki Mima, Kazuo Tanaka, Ryosuke Kodama, Yasuhiko Sentoku and Tatsuhiko Yamanaka [1]

1. INTRODUCTION

To demonstrate the feasibility of the fast ignitor scheme,[1,2] a 100 TW Petawatt Module laser (PWM) was illuminated onto an uniformly imploded spherical shell target. The neutron yield is enhanced from below 10^5 up to 10^6 for the first time and agree with those estimated from the simultaneously detected high energy deuteron yield and spectrum.. A few hundred keV deuterons collide with the cold deuterons in core. Without PWM, no neutrons are observed above the detection threshold of 10^5.

A 60 TW GEKKO Module Laser(GMII laser) was illuminated on plastic foils. CR-39 film stacks measured the energy and angular distribution of the protons emitted from the rear surface of the plastic foils. The ring structure of proton emission leads us to that a toroidal magnetic field associated with the hot electrons work on the fast ions and deflect them. From the logarithmic slope of the ring diameter versus the ion energy, the product of the magnetic field × the length over which it works on the ions is estimated to be up to 1000 MG·μm. The simulation shows that a strong toroidal magnetic field makes the proton's angular distribution to have a similar logarithmic slope.

The 100 TW Petawatt Module Laser (PWM), constructed in 1997,[3,4] is up graded to the world biggest Petawatt Laser (say PW Laser). The PW Laser is to be used for the proof of principle of the scheme and as well for many ultra-intense field reseraches.

2. 100 TW PWM LASER ILLUMINATION ON IMPLODED CD SHELL AND NEUTRON ENHANCEMENT

A target, 500 μm in diameter and 7 μm in thickness, is preimploded by 12 green beams from the GEKKO XII laser. The wavelength is 527 nm and the energy is 2.3 kJ in 2.2 ns Gaussian shape. The 12 beams are focused tangentially onto the target through the random phase plates. At the maximum compression timing, which a fluid code ILESTA-1D[5] predicted to be 2.9 ns after the pulse rise, illuminated is the PWM laser, whose wavelength is 1053 nm, and energy is 90 J on target, respectively. The pulse is the Gaussian of 800fs in FWHM. A parabollic mirror of f-number of 3.5 focused the PWM laser at a point about 200μm from the target center. The critical density point corresponding to the 1μm light is 110 μm from the center. The experimental set up is shown in Fig.1. To detect the D-D neutrons, a plastic(BC-422) scintillator is fully collimated and set at 3.0 m from the target and 40 degrees back to the PWM laser focusing. Figure 2 shows a typical neutron time of flight signal through a numerical noise filter. The spectrum scatters around 2.45 MeV, which shows the feature that the

[1]Yoneyoshi Kitagawa, Kunioki Mima, Kazuo Tanaka, Ryosuke Kodama, Yasuhiko Sentoku and Tatsuhiko Yamanaka, Institute of Laser Engineering, Osaka University,Yamada-oka, 2-6, Suita, Osaka, 565-0871, Japan

Advanced Diagnostics for Magnetic and Inertial Fusion, Edited by Stott *et al.*
Kluwer Academic/Plenum Publishers, New York, 2002

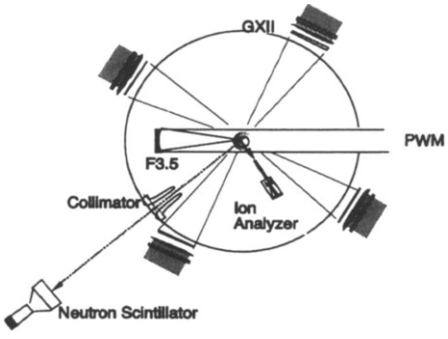

Figure 1. Experimental set for 100 TW PWM laser onto the GXII 12 beam-imploded CD shell target.

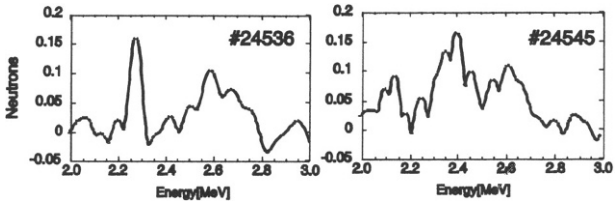

Figure 2. Neutron time of flight signals after a numerical filtering for #24536 (PWM 71 J and GXII 2.2 kJ) and #24545 (86 J and 2.3 kJ) show a beam fusion feature.

energetic deuteron flows collide with dense but cold deuterons in CD plasmas. From the figure, we estimate the averaged spread of the beam to be 25 ± 15 keV for #24545(Fig. 2). Without PWM laser, we have observed no neutrons above the detection threshold of 10^5. As increasing the PWM laser energy, the neutron yield linealy increases. To simultaneously detect the deuteron emissions, a magnetic analyzer with CR-39 film is set 60 degrees forward the laser. The pinhole of Ta is set at 24 cm and the film at 40 cm from the target. After 1 hour etching in 6N NaOH the pit size on the CR- 39 film becomes $3 \sim 5\mu$ m, which comes from keV to MeV deuterons.[6]

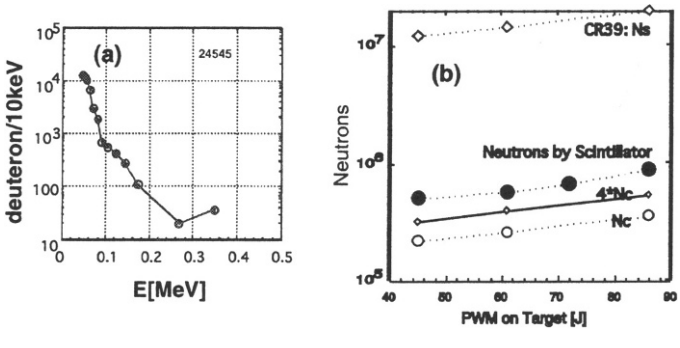

Figure 3. (a) Deuteron spectrum for #24545. (b) Neutron yield comparison between direct scintilaltion data and those estiamted from deuteron emissions for the 1μm critical density N_c, the green light critical $4 * N_c$, and the solid N_s.

Figure 3(a) is the deuteron spectrum for the same shot as Fig. 2. The vertical scale is the particle number/10 keV coming into the detector. The logarithmic temperature is around 20 keV. From the spectrum in Fig. 3(a), we have setimated the neutron yields and compared with those from the plastic schintillator, which is plotted in Fig. 3(b). We set three radial points, at which the laser generates and emits the deuterons in 4π radian. The points are the red light critical density N_c, the green light critical, that is, $4 * N_c$, and the solid N_s. For each case, we estimated the ion stopping power, fusion cross section and the resulting neutron yield. The plots at $4 * N_c$ are close to the scintillator yield , as in Fig. ??. This may lead to that the PWM laser-generated deuteron beams interact with the cold deutrons within the 4× critical density sphere.

3. PROTON REAR EMISSION AND MAGNETIC FIELD GENERATION FROM GMII LASER ILLUMINATED PLASTIC FOILS

Here presented are the observation of proton rear emission and gigagauss scale magnetic fields from 60 TW laser illuminated plastic target. The results are in a good agreement with a two-dimensional PIC simulation.[16] The GEKKO MII CPA laser, used here, produces 25 J at 1.053 μm with 0.45 ps pulse length.[17] The laser pulse, with diameter 140 mm, was focused onto a C_8H_8 target of 3 mm square with an f/3.8 off axial parabolic mirror. 68% of the beam energy was deposited in a spot size of 25 μm in diameter. The target was positioned at 40° to the axis of laser propagation for p-polarization. The intensity on target was $(5.5\pm0.3)\times10^{18}$ W/cm^2. The intensity contrast ratio was 10^3. A one-dimensional hydro code ILESTA-1D[5] predicts a pre formed plasma with a density scale length of 10 μm in the vicinity of the critical density, when the main pulse hits the target. Behind the target, at a distance L of 30 mm and aligned with the normal to the target we placed a 7.5 μm-thick tantalum filter and a stack of four 175 μm thick CR-39 plastic track detectors of 60 mm in diameter, as in Fig. 4.[18–20] Since the tantalum filter stops both carbon ions of less than 10 MeV and protons less than 1 MeV,[21] almost all the tracks on the CR-39 films will be from protons.

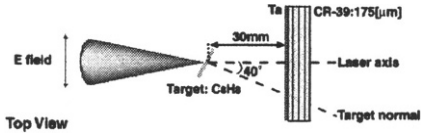

Figure 4. CH target and CR-39 track detector setup. Target is 3-mm square in size and 5 to 100 μm in thickness. CR- 39 film, stack of four layers, covered with Ta foil, is 6 cm in diameter, and is put 3 cm apart from target.

Figures 5 (a) to (d) show the proton tracks on four layered films from 5 μm-thick target after 4 hour etching and Figs. 5 (e) to (h) from 100 μm target. Both the photographs show coaxial ring structures around the target normal axis. Figures 5 (e) and (f) clearly show the ring with a white belt due to much concentration of big pits. For the thickness of 5 and 25 μm, no changes are observed either on the ring structure or emission direction, except that the track number is somewhat reduced for 25 μm. For 100 μm target, large reductions of the track number and ring size are observed. Since a CR-39 film, as well as a Ta foil, is an energy filter, the stacking can analyze the energy of injected ions. The tracks on the first film indicated by (a) and (e) are due to protons of ≥ 1 MeV, the second film due to > 4.8 MeV protons ((b) and (f)), the third > 6.7

MeV ((c) and (g)), and the fourth > 8.2 MeV ((d) and (h)), respectively. The diameter of track pits is again a function of proton energy.[19] So that the energy from the track diameter and the stopping energy on each stack are combined to determine the proton spectrum over the range up to 10 MeV.

The low energy protons will be distributed all over the rear hemisphere. We have summed up the pit number over the film for each energy range and plotted it in Fig. 6 as a function of beam energy. Solid circle is the data for 5 μm target, triangle is for 25, and diamond is for 100. Plots show exponential decay up to 7 or 8 MeV and then a sharp cut off seems to exist around 10 MeV. As the thickness is increased from 5 μm to 25 and 100 , the slope temperature of the spectrum decreases from 3.39 to 3.04 and further to 2.08 MeV, where the slope is given from the exponential curve best fitted to each data line. The yield decreases from 1.8× to 1.2× and to 0.8×10^9, respectively. The protons less than 1 MeV are filtered out by the Ta filter. The PIC simulation will discuss the energy slope and cutoff in a later section. Suppose the protons are generated on the front surface and are transported through the solid plastics (CH) to the rear side. They must loose their kinetic energy inside the solid, leading to a change of the spectrum shape. We can assume a spectrum on the front surface being close to the 5 μm-target spectrum (solid circle in Fig. 6). Then, using this spectrum as the initial value, we calculated the output spectrum on the rear surface of a 100 μm CH, which is plotted by the open circle in Fig. 6. As expected, the temperature increases to 3.6 MeV and the plot is between 5 and 25 μm plots, apparently not close to the 100 μm data(the calculated yield is twice), leading us to believe that the protons are generated not on the front side but on the rear side.

The track pits apparently show ring structure on each film, as in Figs. 5. Almost same energy particles concentrate on the film to make ring structure pits, looking like white circular belts. We assume that a toroidal magnetic field, associated with the hot electron current, deflects proton beams as to form ring structure around the hot electron axis. The diameter d of rings on the film gives the deflection angle θ, as $d = 2L' \tan\theta$, where L' is the distance from the target to CR-39 in the target normal direction, namely, $L' = L/\cos 40°$. The θ is plotted in Fig. 7. The vertical error bar corresponds to the ring width, that is, the width of the white circular belt in Figs. 5. Far right 10 MeV data are from the radius

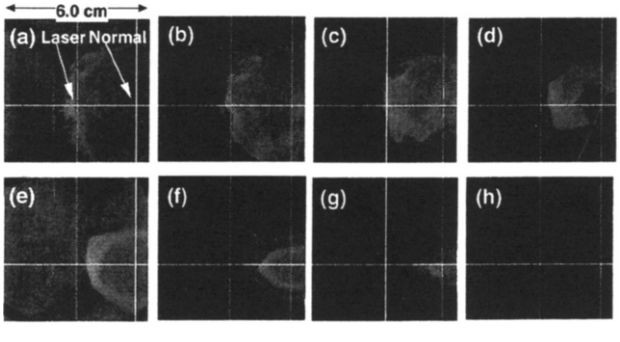

Figure 5. Proton tracks on CR-39 film from 5-μm target (upper (a) to (d)) and 100-μm (lower (e) to (h)): (a) the first film showing the protons of 1 ~4.8 MeV, (b) the 2nd, 4.8 ~ 6.7 MeV, (c) the 3rd, 6.7 ~ 8.2MeV, and (d) the 4th, 8.2 ~ 9.4 MeV. Laser axis is in the center of film and target normal is in the center of track ring. Film aperture is 6 × 6.5cm. Laser is 5.3×10^{18}W/cm^2 on C_8 H_8 target for 40° p-polarization.

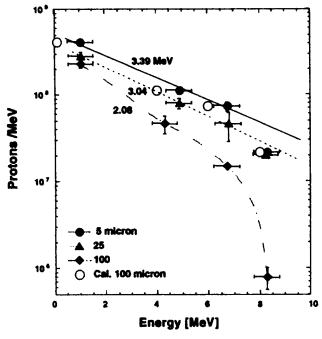

Figure 6. Proton's spectra for the different target thickness ;5 μm (solid circle), 25 μm (triangle) and 100 μm (diamond), respectively. Protons less than 1 MeV are filtered out. Open circle corresponds to 100-μm-thick target, calculated from 5-μm data.

inside the white ring on the final film. A proton gyro radius ρ is given by a magnetic field B_θ and a proton energy $\bar{E}_i$ as

$$\rho[\mu\text{m}] = 1.43 \times 10^3 \bar{E}_i^{1/2}[\text{MeV}]/B_\theta[\text{MG}]. \tag{1}$$

Suppose D is the proton path length in the magnetic field and D is given by $D = \rho\theta$. Also since the proton is accelerated from zero to the final velocity $\bar{E}_i^{1/2}$, when it passes through the magnetic field, we assumed its averaged velocity, $\bar{E}_i^{1/2} \sim E_i^{1/2}/2$. Then

$$\theta[\text{rad}] = \tan^{-1}\left(\frac{d}{2L'}\right) = \frac{B_\theta \cdot D}{1.43 \times 10^3} \cdot \frac{2}{E_i^{1/2}}, \tag{2}$$

where E_i is in the unit of MeV and B_θ in MG, D in μm. The logarithmic slope of the 5 and 25 μm data in Fig.7 equal -1/2 in agreement with that shown in Eq. 2. Figure 7 says that the magnetic fields deflect the protons into a ring structure. Fitting a curve described by Eq. 2 gives the coefficient $B_\theta \cdot D \sim 1000$MG·$\mu$m for these thick targets. For 100 μm thick, the fitting, though it is somewhat poor, yet yields about 500 MG·μm. Square plots in the figure are from the two dimensional (2D) particle simulation (PIC) and the slope is also close to -1/2.

The acceleration of ions during the interaction between the target plasma and the ultra intense laser pulse is studied with the 2D PIC simulations. The following are the simulation parameters; the simulation box is 40 μm $\times$10 μm with a fully ionized DH target plasma, whose thickness is 5 μm, placed at 17.2μm. The maximum electron density is 40 times higher than the critical density n_c of 1 μm laser light. In front of the target, there are preformed plasmas, whose scale length near the critical density is about 7 μm and whose density profile is the exponential profile: $0.2 - 1.2n_c$, respectively. This preformed plasma was prospective in the GEKKO MII experiments as discussed in Sec. II. Note here that the target is initially fully ionized and use a DH plasma to simulate the CH one. The acceleration of the fully ionized carbon C^{6+} and the deuteron D^+ is equivalent due to the same charge/mass ratio.

The p-polarized laser irradiates the target normally from the left boundary. The normalized vector potential a_0 is equal to 3.0, which corresponds to the peak intensity $8 \cdot 10^{18}$ W/cm^2. The total pulse duration is about 400 fs. The pulse rises in 50 fs with half-gaussian profile and keeps the intensity during 300 fs, then

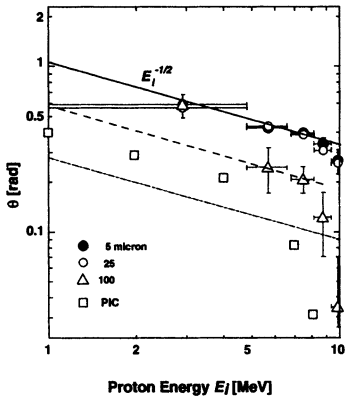

Figure 7. Deflection angle θ of protons versus proton energy. Solid and broken lines from Eq.2 fit to 5 and 100 μm thick target data, respectively. The squares and the dot-broken line are from the 2D PIC simulation.

damps in 50 fs. The transverse profile is also gaussian and its spot size is set to 4μm. The simulation continued 150 fs after the pulse was switched off to see the final proton energy. The total simulation time is 560 fs. Through the simulation, about fifty five percent of the incident laser energy was absorbed in the plasma.

The 2D-PIC simulation shows that the incident laser is reflected at the target surface, then the incident and reflected laser lights are overlapped in the preformed plasma and formed the standing waves. The periodic patterns due to the standing waves are observed in front of the target. Also the very intense positive fields were excited at the target rear side. The maximum E_x, about $0.4 \cdot E_{y0}$, appears at $t = 132$ fs in a few micron scale length. The acceleration energy of this electrostatic field is up to about 5 MeV/μm. Then the E_x expands with expansion of ions. The electrostatic fields at the target rear side have multiple peaks in the case of multiple species plasmas as discussed in Ref.[24] And each peak appears at the expansion front of each ion species. Since the lighter ion is faster than the heavier one, so the first peak appears at the proton expansion front and the second appears at the deuteron front in this simulation.

Quasistatic magnetic fields B_z are caculated both at $t = 198$ fs and 462 fs. In the preformed plasma, bi-pole magnetic fields is driven by the forward accelerated. The intensity is over twenty percent of the laser magnetic field B_{z0}, ~60 MG. At the laser irradiated surface, the magnetic filaments grow from the Weibel instability.[22] The filaments however are localized near the irradiated surface and their intensity is rather weak. Also B_z at the target rear side is still weak, about a few MG, and extended in a several micron at this time (198 fs). Later with plasma expansion, B_z at the target rear side strengthens and extends in the wide region. The time evolution of B_z will be discussed later in this section.

The proton distribution angle in the 2D PIC simulation is smaller than that of the experimental observations. The difference is about factor 2. The evaluated the product of the magnetic field $\times$ the length is $B_z \cdot D \sim 0.1 \cdot B_0 \times 8\mu$m= 240MG$\cdot\mu$m. We could attribute this disagreement of the proton distribution angle in the simulation and in the experiments to the difference of the laser pulse duration. The GEKKO MII laser pulse length is about 100 fs longer than that of this 2D PIC simulation (300 fs). The longer pulse increases both the length and

intensity of the magnetic fields. Also the transverse electrostatic fields E_y expand the ion angular distribution. These E_y's effects were not taken into account correctly in the simulation due to the small scale and periodic boundaries in the transverse space, especially at the later time.

It is found that the high energy protons (> 7 MeV), which go ahead of the deuteron expansion front, feel less magnetic fields and have different angular dependence, that is the high energy protons distribute in wider angles. This angular divergence is explained by the transverse electrostatic fields. This simulation result implies the protons observed in the experiment of the 5 μm target, are the lower energy parts behind the expansion of the deuteron, since their angular distribution just fits on the scale $E_i^{-1/2}$, as in Fig. 7. If the measurement range of the proton energy is extended over 10 MeV, we must check this and see the energy cut-off.

4. PETAWATT LASER CONSTRUCTION

The PWM is up graded to the world biggest Petawatt Laser (PW Laser). Remaining the main amplifier system as it is, we have up-graded the front end, the compressor and the focusing optics of the PWM. The beam size is enlarged from 20 cm to 50 cm to extract 1 PW or 500 J in 0.5 ps.

We have fixed the parameters according to the database of the PWM laser[4] and the related fast ignitor experiments.[2]

The front end has newly introduced an optically parametric chirped pulse amplifier (OPCP Amplifier) to suppress prepulses. A 40-cm diam. deformable mirror compensates phase distortions on the beam cross section. The final beam size is 50 cm. A pair of 1-m diffraction gratings, set in double path configuration, compresses the pulse length into 500 fs. The PW laser is synchronized to the GEKKO XII beams within 10 ps. As shown in Fig.8, the compression chamber is put on an iron frame at the heigh of 7.16 m from the room floor. To suppress vibrations of optics inside the chamber, the frame is made of a 25 cm ×25 cm squared column.

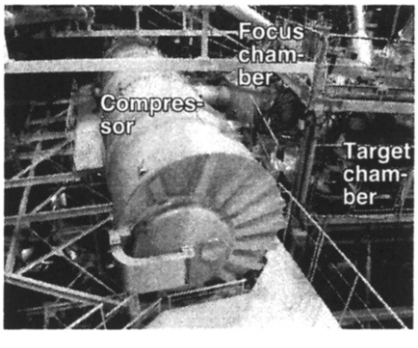

Figure 8. Compressor, focusing and target chambers.

An off-axial parabola mirror of 3.8 m focal length (the F-number is 7.6) provides the intensity of 2×10^{20} W/cm^2 or more on target. The focusing system is installed in a vacuum chamber of 2.2 m in diameter and 1.18 m in height. The chamber is connected through a gate valve to the horizontal 8 inch port of the target chamber.

5. CONCLUSION

The PWM laser has illuminated the CD shell target, imploded by GXII twelve beams. The laser-generated deuteron beams interact with the cold deutrons within the 4× critical density sphere and enhance ten times the D-D neutron yield.

The energetic protons, emitted from the rear surface of the ultra-intense laser illuminated CH foils. The protons are dragged away from the rear surface, where the hot electrons formed a virtual cathode. For 5 (and 100) μm thick target, 1.8 (and 1.2) $\times 10^9$ protons have an average energy of 3 (and 2) MeV. Coaxial ring structure of protons shows $B_\theta \cdot D$ to be 1000 (500) MG·μm. The 2D PIC simulation is close to the experiment. The energetic protons originate from the rear side acceleration. The magnetic fields grew and extended with the plasma expansion at the target rear side. These toroidal quasistatic magnetic fields, whose intensity is up to several tens megagauss, defocus the proton beams.

The world biggest Petawatt Laser has constructed. The out put is 1 petawatt, which is used also for ultra-intense laser matter interactions above the intensity of 10^{20} W/cm^2.

REFERENCES

1. M. Tabak, J. Hammer, M. E. Glinsky, W. L. Kruer, S. C. Wilks, J. Woodworth, E. M. Campbell, M. D. Perry, and R. J. Mason, **1**, 1626 (1994).
2. K.A. Tanaka *et al.*, Phys. Plasmas **7**, 2014-2022 (2000).
3. Y. Kato *et al.*, Plasma Phys. Controlled Fusion **39**, 1801 (1994).
4. Y. Kitagawa *et al.*, *"Final Report on PWM Laser"*, Institute of Laser Engineering, Osaka University (November 2000).
5. H. Takabe, M. Yamanaka, K. Mima *et al.*, Phys. Fluids **31**, 2884 (1988).
6. M.SADOWSKI *et al.*, Radiation Measurments **28**, 207-210 (1997).
7. A. P. Fews, P. A. Norreys, F. N. Beg, A. R. Bell. A. E. Danger, C. N. Danson, P. Lee, and S. J. Rose, Phys. Rev. Letters **73**, 1801 (1994).
8. E. L. Clark, K. Krushelnick, J. R. Davis *et al.*, Phys. Rev. Letters **84**, 670 (2000).
9. S. P. Hatchett, C. G. Brown, T. E. Cowan *et al.*, Phys. Plasmas **7**, 2076 (2000).
10. S. C. Wilks, A. B. Langdon, T. E. Cowan, M. Roth, M. Singh, S. P. Hatchett, M. H. Key, D. Pennington, A. Mackinnon, and A. Snavely, Phys. Plasmas **8**, 542 (2001).
11. A. Maksimchuk, S. Gu, K. Flippe, D. Umstadter, and V. Yu. Bychenkov, Phys. Rev. Letters **84**, 4108 (2000).
12. A. Puhkov, Z. -M. Sheng, J. Meyer-ter-Vehn *et al.*, Phys. Plasmas **6**, 2847 (1999).
13. E. G. Gamaly, Phys. Fluids **B5**, 3765 (1993).
14. S. Humphries, Jr., *Charged Particle Beams* (John Wiley and Sons, Inc., New York, 1990) Ch. 6 .
15. K. Krushelnick, E. L. Clark, Z. Najimudin *et al.*, Phys. Rev. Letters **83**, 737 (1999).
16. Y. Murakami, Y. Kitagawa, Y. Sentoku *et al.*, to be published in Phys. Plasmas, September, 2001.
17. M.Mori, Y. Kitagawa, R. Kodama *et al.*, Nuclear Instrument Methods in Phys. Research **A410**, 367 (1998).
18. Y. Yamada, Y. Kitagawa, M. Yokoyama, and C. Yamanaka, Phys. Letters **83A**, 9 (1981).
19. A. Szydlowski, M. SAdowski, T. Czyzlwski, M. Jaskofa, and A. Korman, Nuclear Instrument Methods in Phys. Research **B149**, 113 (1999).
20. Y. Kitagawa, K. A. Tanaka, M. Nakai *et al.*, Phys. Rev. Letters **75**, 3130 (1995).
21. J. F. Ziegler, *Stopping and Ranges of Ions in Matter* (Pergamon Press, New York, 1980) Vol. 5.
22. Y. Sentoku, K. Mima, S. Kojima, and H. Ruhl, Phys. Plasmas **7**, 689 (2000).
23. E. Lefebvre and G. Bonnaud, Phys. Review E **55**, 1011 (1997).
24. Y. Sentoku, V. Yu. Bychenkov *et al.* "High energy ion production from short-laser-pulse interaction with high density plasmas" submitted to Phys. Plasmas.
25. Wei Yu, V. Bychenkov, Y. Sentoku, M. Y. Yu, Z. M. Sheng, and K. Mima, Phys. Rev. Letters **85**, 570 (2000).
26. H. Yoshida *et al.*, Rev. Laser Eng. **27**, 291-297 (1999).